Vol. 1, No. 2 (2023) pp 92-105 https://doi.org/10.59535/faase.v1i2.178





# Influence of Zinc Nitrate Tetrahydrate and PLA/Cu<sub>2</sub>O Film on ZnO Nanorods Nanogenerator Performance

Yani Anggraeni <sup>1</sup>, Nandang Mufti <sup>1\*</sup>, Sumera Rafique <sup>2</sup>, Guangda Hu <sup>3</sup>

- <sup>1</sup> Program Studi Fisika, Universitas Negeri Malang, **Indonesia**.
- <sup>2</sup> Department of Physics, University of Balochistan, Quetta, **Pakistan**.
- <sup>3</sup> School of Materials Science and Engineering, University of Jinan, Shandong, **China**.

⊠ yani.anggraeni@student.um.ac.id

## **Open Access**

This article contributes to:





Abstract. ZnO nanorods are a 1-D material that can be used as a triboelectric nanogenerator application to harvest energy from the surrounding environment. This research aims to analyze the effect of the ratio of Zinc Nitrate Tetrahydrate and PLA/Cu2O Film on the morphology, crystal phase and electrical properties of the ZnO Nanorods Nanogenerator. ZnO nanorods were grown on stainless steel substrates using a hydrothermal method. Growth was carried out at a temperature of 100°C for 4 hours with varying concentrations of zinc nitrate tetrahydrate of 40 mM, 50 mM, 60 mM, and 70 mM with a fixed concentration of 40 mM hexamethylenetetramine. The XRD test results of ZnO nanorods obtained a hexagonal wurzite crystal structure with lattice parameters a = b = 3.2446 Å and c = 5.1987 Å. The diameter and length of the ZnO nanorods as a result of SEM characterization are 91.66 nm and 563.8 nm in a sample ratio of 1:1; 76.87 nm and 263.3 nm on a sample ratio of 1.25:1; 87.16 nm and 616.16 nm on a sample ratio of 1.5:1; 73.19 nm and 706.9 nm on a sample ratio of 1.75:1. The results of current and voltage measurements on trielectric nanogenerator devices based on ZnO nanorods and PAN polymer were respectively 4.4 μA, 3.8 V; 26.8 μA, 23.3 V; 8.9 μA. 11.9V; and 9.7 µA, 14.7 V. The results show that the smaller the diameter of the ZnO nanorods, the better the efficiency of the resulting nanogenerator.

**Keywords:** ZnO nanorods, stainless steel, hydrothermal method, triboelectric nanogenerator.

## 1. Introduction

One-dimensional (ID) nanostructures for piezoelectric materials such as ZnO, AlGaN, GaN, InN, PZT, PVDF, TiO2, CdS are widely used to harvest mechanical energy and are environmentally friendly [1], [2], [3]. Among several materials, ZnO is a group II-VI ntype semiconductor material which has technical applications such as photocatalysts [4], solar cells [5], thin gas film sensors [3], nano-piezoelectric, piezoelectric nanogenerators [6]. It can also be applied as a transparent oxide layer in optical devices due to its wide band gap. ZnO also has a wide band gap of around 3.37 eV and an excitonic binding energy of around 60 meV at room temperature and consists of a wurtzite crystal structure with lattice parameters a = 3.248 Å and c = 5.205 Å. ZnO is also a semiconductor material that is considered a promising piezoelectric material that can produce potential voltage through deformation of piezoelectric ZnO nanorods by external forces [7]. Among other materials, ZnO nanostructures can be easily grown at low temperatures on various substrates which are the main functional materials of piezoelectrics because they have physical, chemical and optical properties as well as the advantages of biocompatibility and non-toxicity from the environment [8].

The properties of nanostructured ZnO depend on the size and shape of its structures such as nanowires, nanorods, nanodots, nanotubes, nanosheets, nanobelts, nanoribbons, and nanorings have been considered as one of the most promising materials for manufacturing piezoelectrics because they show high response to piezoelectricity, mechanical properties that good, large aspect ratio, and high electron

Article info Submitted: 2023-11-05

**Revised:** 2024-01-30

**Accepted:** 2024-01-31



This work is licensed under a Creative Commons Attribution 4.0 International License. mobility [9]. The advantage of using ZnO nanorods as energy harvesting is due to its ability to build a piezoelectric potential field within itself [10].

Various techniques used to make ZnO thin films include RF sputtering [11], spray pyrolysis [12], metal organic chemical vapor deposition [13], and sol-gel process [14]. Among other techniques, the sol-gel method is widely used to manufacture transparent oxides because it is simple, safe, does not require an expensive vacuum system, and the method used is very cheap for coating. The sol-gel process also has many advantages such as high surface morphology at low crystalline temperatures, easy control of chemical components, and low-cost thin film formation to investigate the structural and optical properties of ZnO thin films [9].

Among the materials used for Piezoelectric Nanogenerator (PNGs) applications, ZnO is the most widely used semiconductor material because of its polar asymmetric crystal structure which gives rise to piezoelectric properties and easy formation of various forms of nanostructures such as flexible organic, textile, and insulating substrates [15]. For these applications, devices used for self-powering such as stainless steel are very promising because stainless steel is one of the materials that is widely used and has many advantages such as corrosion resistance, mechanical strength, and electrical conductivity. Additionally, stainless steel as a substrate for Piezoelectric Nanogenerators (PNGs) provides a low cost and conductive electrode that allows PNGs to hybridize with other technologies such as batteries and photovoltaics.

Cuprous oxide ( $Cu_2O$ ) is a p-type semiconductor material used for low-cost applications, large-scale solar energy conversion due to its abundant copper and oxygen properties, a band gap suitable for visible light absorption, and effective in energy-intensive fabrication processes low as electrodeposition, so that the semiconductor cuprous oxide ( $Cu_2O$ ) as a Hole Transporting Layer (HTL) has great potential to improve the performance of ZnO nanorods [16].

Various studies that have been carried out in synthesizing ZnO nanorods include using the hydrothermal method using ethanol solvent and transparent conductive glass FTO (Fluorine-Tin Oxide) with varying precursor concentrations and different immersion times, ZnO nanorods with the largest diameter of 82 nm and a length of 100 nm. concentration of 35 mM with an immersion time of 180 minutes at a temperature of 90°C [9]. In the same year, a study also succeeded in synthesizing ZnO nanorods with the largest diameter and length, namely 56 nm and 910 nm at a concentration of 10 mM for 5 hours. The results obtained from ZnO nanorods grown at a concentration of 10 mM for 5 hours were used to test the nanogenerator [17].

Based on the background explained above, to obtain optimization of the formation of piezoelectric film nanogenerators based on ZnO nanorods which are effective in generating potential voltage through deformation of piezoelectric ZnO nanorods with external forces. In this research, the substrate used to grow ZnO nanorods is stainless steel. In growing nanorods, the precursor concentration was varied to determine its effect on the crystal structure, morphology and band gap of ZnO nanorods. This research aims to analyze the effect of the ratio of Zinc Nitrate Tetrahydrate and PLA/Cu<sub>2</sub>O Film on the morphology, crystal phase and electrical properties of the ZnO Nanorods Nanogenerator.

## 2. Method

## 2.1 Procedure for Preparing ZnO Solution and Coating

The ZnO solution is made by dissolving Zn (CH<sub>3</sub>COO)<sub>2</sub>.2H<sub>2</sub>O powder in an ethanol solution. So that the two solutions are mixed perfectly, the mixture is stirred using a

magnetic stirrer on a hot plate at a temperature of 70°C for 45 minutes. Then, Monoethanolamine (MEA) was added little by little to the solution, stirred at a constant temperature of 70°C for 2 hours. The ratio of Zn (CH<sub>3</sub>COO)<sub>2</sub>.2H<sub>2</sub>O: MEA is 1:1. After that, the solution was left at room temperature for 24 hours so that the solution formed was homogeneous and transparent. In ZnO film coating, Stainless Steel (SS) is used as a substart. The clean SS substrate is placed on the spin coater and the ZnO solution is dripped on top of the SS then spun (spinning) at a rate of 3000 rpm for 20 seconds. Preheating at 150oC for 2 hours. The annealing process is carried out in a furnace.

## 2.2 Growing Procedures ZnO Nanorods

After coating the ZnO nanoparticle film on a Stainless Steel (SS) substrate, ZnO nanorods were grown via a hydrothermal method. Growth solution was prepared using Zinc Nitrate Tetrahydrate  $(Zn(NO_3)_2.4H_2O)$ which acts  $Zn^{2+}$ and Hexamethylenetetramine (HMT) ( $C_6H_{12}N_4$ ) in Deionized Water. Varying concentrations of Zinc Nitrate Tetrahydrate precursor used were 50 mM, 70 mM and 90 mM. Meanwhile, Hexamethylenetetramine 35 mM was kept constant. The solution was stirred using a magnetic stirrer for 45 minutes at room temperature. Then, the ZnO film was dipped in the prepared solution. During the growth process, the solution was heated at 90°C for 6 hours. Then the sample was rinsed with DI-Water to remove residual salt from the sample surface and dried with a blower. Finally, the ZnO nanorods on the SS substrate were annealed at a temperature of 550°C for 2 hours in a furnace.

## 2.3 PLA/Cu<sub>2</sub>O coating procedure

In coating the PLA/Cu2O film, Stainless Steel (SS) is used as a substrate, a solution (1) is made, namely 0.55 gram PLA dissolved in 3.55 ml chloroform, then stirred for 1.5 hours at a speed of 350 rpm until homogeneous after that increased to 600 rpm. Solution (2) was made with 0.137 gram  $Cu_2O$  dissolved in 3.55 ml chloroform in a stirrer for 30 minutes. Then solutions (1) and (2) were mixed in a stirrer for 1 hour at a speed of 600 rpm, after which they were sonicated for 3 hours. The mixture of solutions (1) and (2) was spin coated on the SS substrate at a speed of 3000 rpm for 20 seconds. Preheating at  $150^{\circ}C$ , for 10 minutes.

## 3. Result and Discussion

## 3.1 XRD Characterization Results

## 3.1.1 Diffraction Pattern of Zno Nanoparticles

In this research, ZnO nanorods were grown on a Stainless Steel (SS) substrate in two stages, where the first stage was deposited on the substrate using the sol gel spin coating method with pH 7 and the second stage was the growth of ZnO nanorods using the hydrothermal method. These ZnO nanoparticles act as a buffer layer in growth ZnO nanorods.

The x-ray diffraction pattern of ZnO nanoparticle samples with pH 7 is shown in Fig 1. From Figure 1 shows that the crystallinity of ZnO nanoparticles grown on a Stainless Steel (SS) substrate with a pH of 7 is not visible, because this layer is too thin to be illuminated by X-ray Difraction. This light penetrates the ZnO layer that hits Stainless Steel (SS) so that the peaks that are read belong to stainless steel. Based on the XRD results, the peaks of Stainless Steel (SS) are formed at angles of 44.27°, 64.56° and 64.79°. However, at an angle of 32.8°, iron chromium oxide also forms from the Stainless Steel (SS) substrate because SS can resist high temperature corrosion and oxide by dissolving these materials to produce a coherent protective film that adheres, isolates and regenerates chromium oxide on the surface [7].

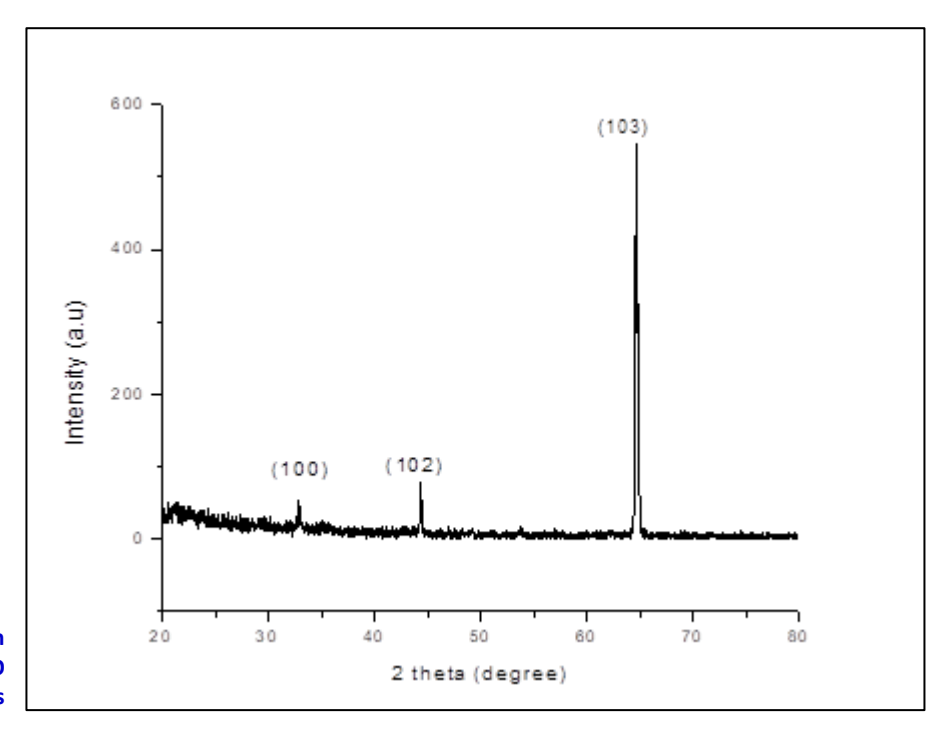


Figure 1 Diffraction
Pattern of ZnO
Nanoparticles

Based on the results of the X-ray diffraction pattern, ZnO nanoparticles with a pH of 7 are in accordance with what was done by Naik et al. [18], who stated that the ZnO diffraction pattern with the highest peak intensity in the (002) plane had good crystallinity using an ITO substrate. ZnO nanoparticles with a pH of 7 were also characterized using SEM to determine the morphology formed in the sample. Next, ZnO nanorods were grown on the samples that had been coated with ZnO.

#### 3.1.2 Diffraction Pattern ZnO Nanorods

The growth of the nanorods structure uses the hydrothermal method with ZnO nanoparticles as the support layer. In this research, the growth of ZnO nanorods was carried out with three variations in the concentration of the Zinc Nitrate Tetrahydrate precursor Zn(NO<sub>3</sub>)<sub>2</sub>.4H<sub>2</sub>O, namely 50 mM, 70 mM, and 90 mM. Meanwhile, the concentration of Hexamethylenetetramine / HMT (C6H12N4) was kept at 35 mM. From variations in concentration, the ratio between Zinc Nitrate Tetrahydrate and Hexamethylenetetramine (HMT) is 1.4:1, 2:1, and 2.5:1. The X-ray diffraction pattern of ZnO nanorods with varying precursor concentrations is shown in Figure 2.

Figure 2 shows the results that the X-ray diffraction peak of ZnO nanoparticles is not visible because the ZnO layer is too thin so that the incoming X-rays penetrate the ZnO layer on Stainless Steel (SS) which can be read by Xray-Ray Difraction (XRD), due to the pores of Stainless Steel (SS) is too small or smooth for the metal to remain shiny. All samples of ZnO nanorods with varying precursor concentrations with Stainless Steel (SS) substrates located in the (100), (002), and (101) planes show that the growth of ZnO crystals is not in one direction but some are oriented in different directions. The crystal orientation of the highest peak intensity is located in the (002) plane which is located between angles of 34.14°-34.49°.

However, at a ratio of 2:1 at an angle of  $29.8^{\circ}$ , iron chromium oxide is formed and at an angle of  $35.2^{\circ}$ ,  $Fe_2O_3$  (hematite) is formed. This compound comes from the 304 L stainless steel substrate because SS can withstand high temperature corrosion and oxide by dissolving the ingredients. This material produces a coherent protective film, adheres to, isolates and regenerates chromium oxide on the surface [11], [16]. Similarly, with a ratio of 2.5:1 at an angle of  $29.8^{\circ}$ , iron chromium oxide is formed, an angle of 35.080 is formed by  $Fe_2O_3$  (hematite), and an angle of  $44.5^{\circ}$  belongs to the top of stainless steel.

From Figure 2 it can be seen that at a ratio of 2:1 and a ratio of 2.5:1 the peak of stainless steel (SS) is still read by X-Ray Diffraction (XRD) perhaps because the ZnO layer has gaps that can penetrate SS.

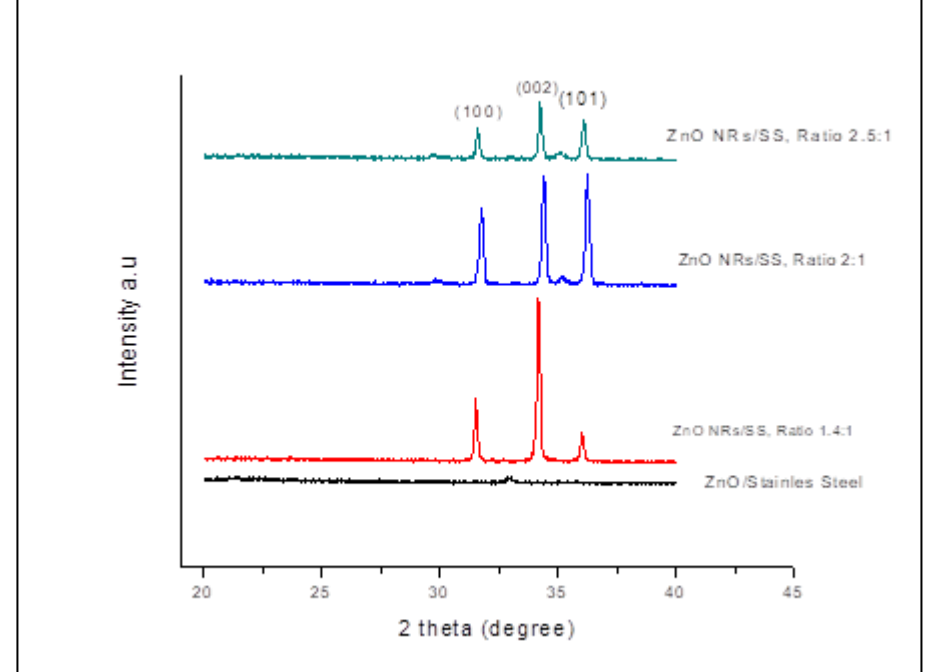


Figure 2 Diffraction
Pattern of ZnO
Nanorods with
Varying Precursor
Concentrations on
the ZnO
Nanoparticle/Stainl
ess Steel (SS)
Support Layer

The diffraction pattern in Figure 2 is in accordance with research conducted by Mufti et al. [15] which states that the highest peak of ZnO nanorods is located in the (002) plane at an angle of 34.22°-34.45°. It was observed that, the deposited film was polycrystalline with a hexagonal wurtzite structure with the highest orientation along the c-axis and perpendicular to the substrate surface [19].

From the results of The highest peak intensity in all samples was obtained at a ratio of 1.4:1. Good crystal quality is characterized by a small FWHM (Full Width at Half Maximum) value and a fairly large crystal grain size. The smaller the crystallinity size, the wider the resulting diffraction peak. Large crystals with one orientation produce diffraction peaks that approach a vertical line. Very small crystallinity produces very wide diffraction peaks. The width of the diffraction peaks provides information about the size of the crystallinity. Thus, the crystal grain size or crystal structure can be determined through x-ray diffraction pattern analysis using Scherrer's method which will be discussed in the next analysis.

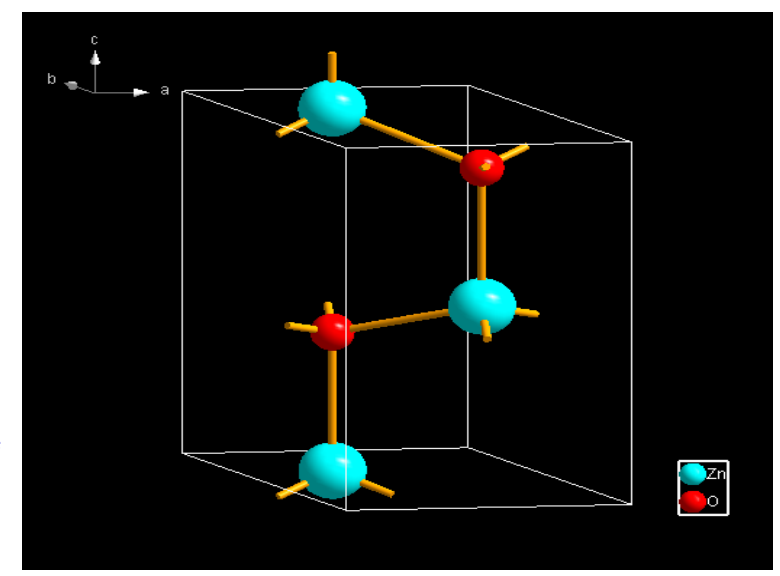
## 3.1.3 Crystal Structure ZnO Nanorods

Based on the XRD characterization results, the crystal structure of the X-ray diffraction pattern of ZnO nanorods was analyzed using Rietica software with the Rietveld refinement method. The results of data analysis are shown in Table 1.

Table 1. Crystal Structure of ZnO Nanorods

Parameter	ZnO NRs/SS Ratio 1.4:1	ZnO NRs/SS Ratio 2:1	ZnO NRs/SS Ratio 2.5:1
a=b(Å)	3,2413	3,2563	3,2678
c (Å)	5,1954	5,2186	5,2364
c/a <sub>o</sub>	1,602	1,602	1,602
V(Å <sup>3</sup> )	47,244	47,92	48,42
GoF(%)	1,42	2,27	1,79
Rwp	20,85	26,39	27,42
Rp	15,93	19,73	19,77
Rexp	17,49	17,50	20,48

The results of the crystal structure analysis in Table 1 show that the lattice parameters for all samples have a c/a ratio of 1.6. The results of this research are in accordance with the results carried out by Jayababu and Kim [7] that the wurzite crystal structure has a hexagonal unit cell with two lattice parameters a and c, having a c/a ratio of around 1.6. This shows that the structure of the ZnO nanorods formed in this research is hexagonal wurtzite. The crystal structure model based on the lattice parameters of the ZnO nanorods formed can be visualized using Diamound software. This software can be used to determine the Wyckoff position of ZnO, and the shape of the crystal structure model can be clearly identified. The visualization results are depicted in Figure 3.



It can be seen that the crystal structure formed in all ZnO nanorods samples proves the results of the previous analysis, namely formation the of hexagonal wurtzite structure with the crystal orientation pointing towards the c-axis. for the Wyckoff position of the ZnO atom is shown in Table 2.

Figure 3.
Visualization of ZnO Nanorods
Crystal Structure
Model

Table 2. ZnO Atom Parameters

Atom	Wyck.Pos	X	Υ	Z
Zn	2 b	1/3	2/3	0
Ο	2 b	1/3	2/3	0,3821

To determine the crystal grain size of ZnO nanorods, the X-ray diffraction pattern of each sample was analyzed using the Scherrer's equation with origin8 software. The results of the analysis are presented in Table 3.

Table 3. Results of ZnO Nanorods Crystal Grain Size with Formula Scherrer's

Ratio comparison	Grain size (nm)	FWHM
Ratio 1.4:1	50,04	0,17817
Ratio 2:1	43,2	0,19938
Ratio 2.5:1	51,2	0,17502

The crystal size of the ZnO nanorods produced at a 1.4:1 ratio was 50.4 nm, a 2:1 ratio was 43.2 nm, and a 2.5:1 ratio was 51.2 nm. The ratio comparison above uses varying concentrations of Zinc Nitrate Tetrahydrate, namely 50 mM, 70 mM, 90 mM using a Hexamethytetramine (HMT) constant of 35 mM. It can be seen that there is a decrease in crystal size from a ratio of 1.4:1 to a ratio of 2:1, while from a ratio of 2:1 to a ratio of 2.5:1 the crystal size increases. Based on analysis of x-ray diffraction patterns, this is because the smallest FWHM value is at a ratio of 2.5:1, so that the crystal grain size at this ratio has the largest crystal grain size compared to other samples (attachment 5).

Based on research conducted by Bowmaker et al. [20], who used variations in the concentration of Zinc Nitrate Tetrahydrate in the growth solution to be high, the ZnO nanorods formed will be faster with low porosity in ITO/PET because they are synthesized in isotropic growth due to the higher amount. from Zn<sup>2+</sup> ions. The diameter depends on the size of the crystal grains, the larger the grain size, the larger the resulting diameter

[21]. Precursor concentration is a factor that influences the size and morphology of crystals, this is due to critical diffusion of monomers, growth limitations, deposition conditions, and surface tension in the dyeing process. However, in this study the largest crystal grain size was obtained in ZnO nanorods with a ratio of 2.5:1. This is possible due to the influence of temperature control during growth, because the temperature control equipment used is very simple. Changes in temperature during growth can change the FWHM value and the average size of crystal grains.

#### 3.2 SEM Characterization Results

## 3.2.1 SEM characterization results of ZnO nanoparticles

The surface morphology formed on the sample can be determined through SEM characterization results.

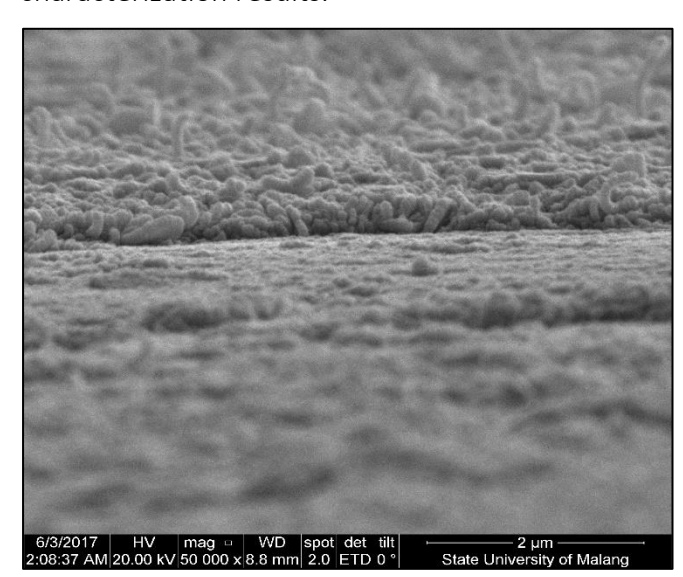


Figure 4 shows the surface morphology of the ZnO film with pH 7 used as a medium for growing nanorods. The concentration ratio between Zinc Acetate Dihydrate and Ethanol carried out in the synthesis process is 1:1. Based on the results of XRD and SEM analysis, this sample was used as a buffer layer in the growth of ZnO nanorods.

Figure 4. SEM results of ZnO/SS Thin Film

## 3.2.2 SEM Characterization Results of ZnO Nanorods

The results of SEM characterization of ZnO nanorods with varying precursor concentrations in Zinc Nitrate Tetrahydrate with the HMT constant are shown in Figures 5 and 6.

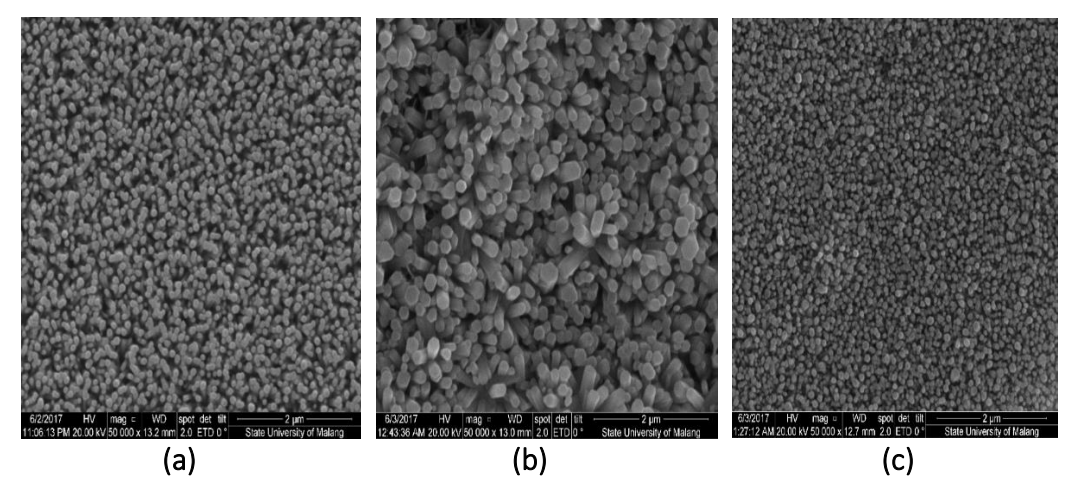


Figure 5.
Characterization
Results of ZnO
Nanorods/SS Film
with Ratio
Comparison of a)
1.4:1, b) 2:1, c)
2.5:1 at 100kx
Magnification

Based on Figure 5, the SEM characterization results of ZnO nanorods show the formation of a rod-shaped structure with a hexagonal structure on the entire surface of the substrate, where each anion is surrounded by four cations at the corners of the tetrahedrant. All samples of ZnO nanorods with a variety of precursors with Stainless Steel (SS) substrates show that ZnO crystal growth is not in one direction but some are still oriented in different directions. Among the other samples, the sample with a ratio of

1.4:1 (Figure 5.a) shows the best growth of ZnO crystals oriented in one direction among others. This is possible due to the influence of deposition conditions and stress on the dyeing process.

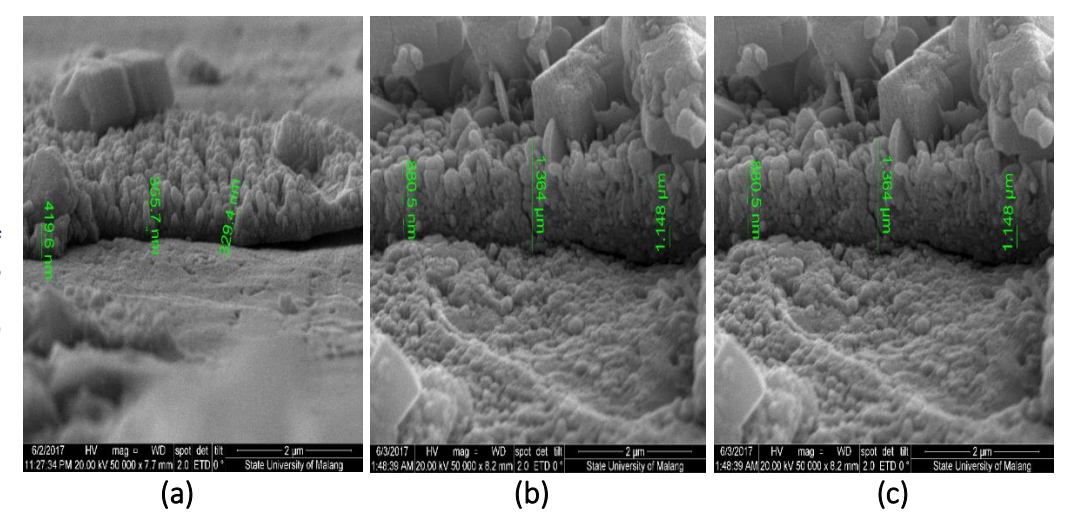


Figure 6. Results of ZnO Nanorods/SS Film Characterization with Ratio Comparisons of a) 1.4:1, b) 2:1, and c) 2.5:1 seen from the Cross Section

Figure 6 shows the average film thickness obtained from the SEM results of the cross-section, which is tabulated in Table 4.

Table 4. Average thickness of ZnO Nanorods Film

Thickness	ZnO/SS (μm)	ZnO Nanorods/SS (μm)		
	Z110/33 (μ111)	Ratio 1,4:1	Ratio 2:1	Ratio 2,5:1
1	0,3089	0,4196	1,259	0,8805
2	0,3792	0,3557	1,154	1,364
3	0,3789	0,3294	1,032	1,148
Average	0,356	0,3682	1,1483	1,1308

From the data in Table 4, the average thickness obtained for the ZnO nanorods samples is thicker than that of ZnO nanoparticles. The thickness of ZnO nanorods at each variation of precursor concentration is not the same. The largest film thickness of ZnO nanorods was obtained at a ratio of 2:1. It is possible that there are differences in the deposition conditions of the precursor solution during the growth process. Thus, the deposition conditions of the precursor solution can affect the film thickness. To determine the average diameter and length of ZnO nanorods, the SEM characterization results were analyzed using ImageJ software. The measurement results are presented in Table 5 below.

Table 5. Length and Diameter of ZnO Nanorods

Ratio comparison	Length (nm)	Diameter (nm)
1,4:1	386.606	81.568
2:1	774.020	115.800
2,5:1	339.940	80.429

In Table 5 it can be seen that the lengths of nanorods with ratios of 1.4:1, 2:1, 2.5:1 are 386.6 nm, 774.0 nm, and 339.9 nm respectively and their diameters are respectively 81.56 nm, 115.8 nm, and 80.8 nm. This is possible due to the influence of differences in substrate position on the nanorods growth process. Based on theory, nanorods are a form of rod-shaped nanostructure with a dimensional diameter range of around 1-100 nm which is called a nano regime [8]. Thus, in this research, ZnO nanorods films that have a diameter above 100 nm are ZnO nanorods with a ratio of 2:1.

## 3.3 Dielectricity Test Results

Characterization of dielectricity measurements on samples of ZnO nanorods, PLA film, and PLA/Cu2O film using an LCR meter showed that the measurement results were

capacitance (C), cross-sectional area (A), distance between plates (d), and air permittivity  $\varepsilon o=8$ ,  $85 \times 10^{-12}$  F/m can be done to find the dielectric constant ( $\varepsilon^{\Lambda}$ ') with the following equation.

$$\varepsilon' = \frac{cd}{\varepsilon_0 A} \qquad (1)$$

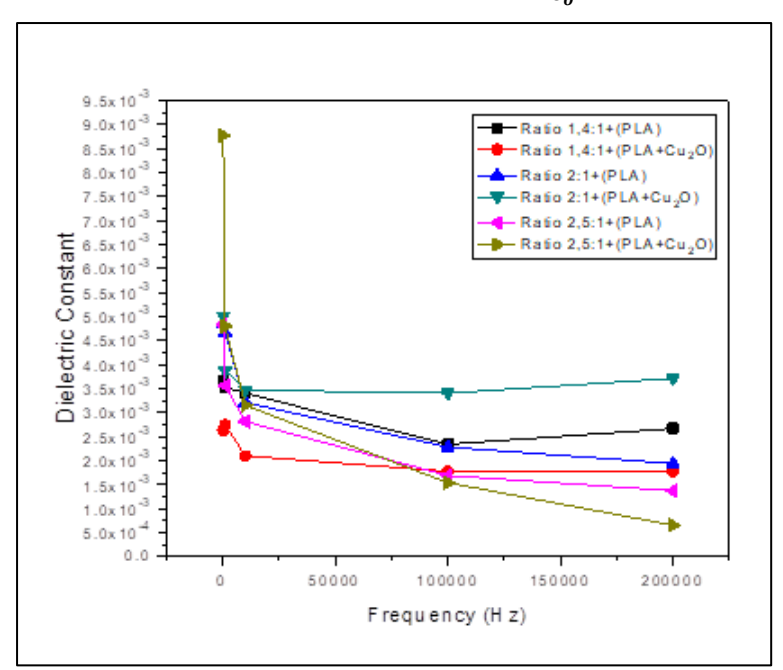


Figure 7. Relationship between Frequency (Hz) and Dielectric Constant

Figure 7 shows the relationship between the dielectric constant value and the given frequency. The greater the frequency, the dielectric constant decreases. This is because the dielectric constant value is inversely proportional to frequency. The frequency range is 100000 Hz- 200000 Hz at a ratio of 1.4:1+(PLA) and ratio 2:1+(PLA+Cu2O). The dielectric constant value tends to be random, this is because the polarization

ability of the dielectric material changes according to the given frequency. Dielectric materials that are subjected to low frequencies produce varying values that will appear random. This is because at low frequencies the dipole moment is opposite to the electric current. The dielectric constant value decreases at high frequencies because the dipoles receive torsion forces which cause them to align themselves with the electric field. Dielectric properties are properties that describe the level of ability of a material to store electric charge at a high potential difference. Dielectric properties are often associated with the electrical insulator material placed between the two capacitor plates. If an insulating material is subjected to an electric field placed between the two capacitor plates, an electric dipole is formed within the material. So that on the surface of the material an induced electric charge can occur (Sutrisno and Gie, 1983).

## 3.4 I-V characteristics of Piezoelectric Nanogenerators

#### 3.4.1 Current Characteristics (I)

I-V characteristics of the piezoelectric nanogenerator device, this measurement is carried out by pressing using regular mechanical force and relaxation. The mechanical strength per area is measured and the results are shown in Figure 8. Figure 8 shows the relationship between current and time in the piezoelectric nanogenerator device of ZnO nanorods film, PLA film, and PLA/Cu<sub>2</sub>O film. An electrometer is used to measure current, while an oscilloscope is used to measure voltage. The response obtained from the nanogenerator due to the dynamic force of the impact of a given human finger/hand can be seen in Figure 8. The maximum current obtained reaches 85 nA at a ratio of 1.4+(PLA). The output current produced by the performance of the nanogenerator using PLA film shows a good response compared to using PLA/Cu<sub>2</sub>O film (Table 6), this is in accordance with the voltage produced which shows a good response using PLA film compared to PLA/Cu<sub>2</sub>O film which can be seen in Table 7.

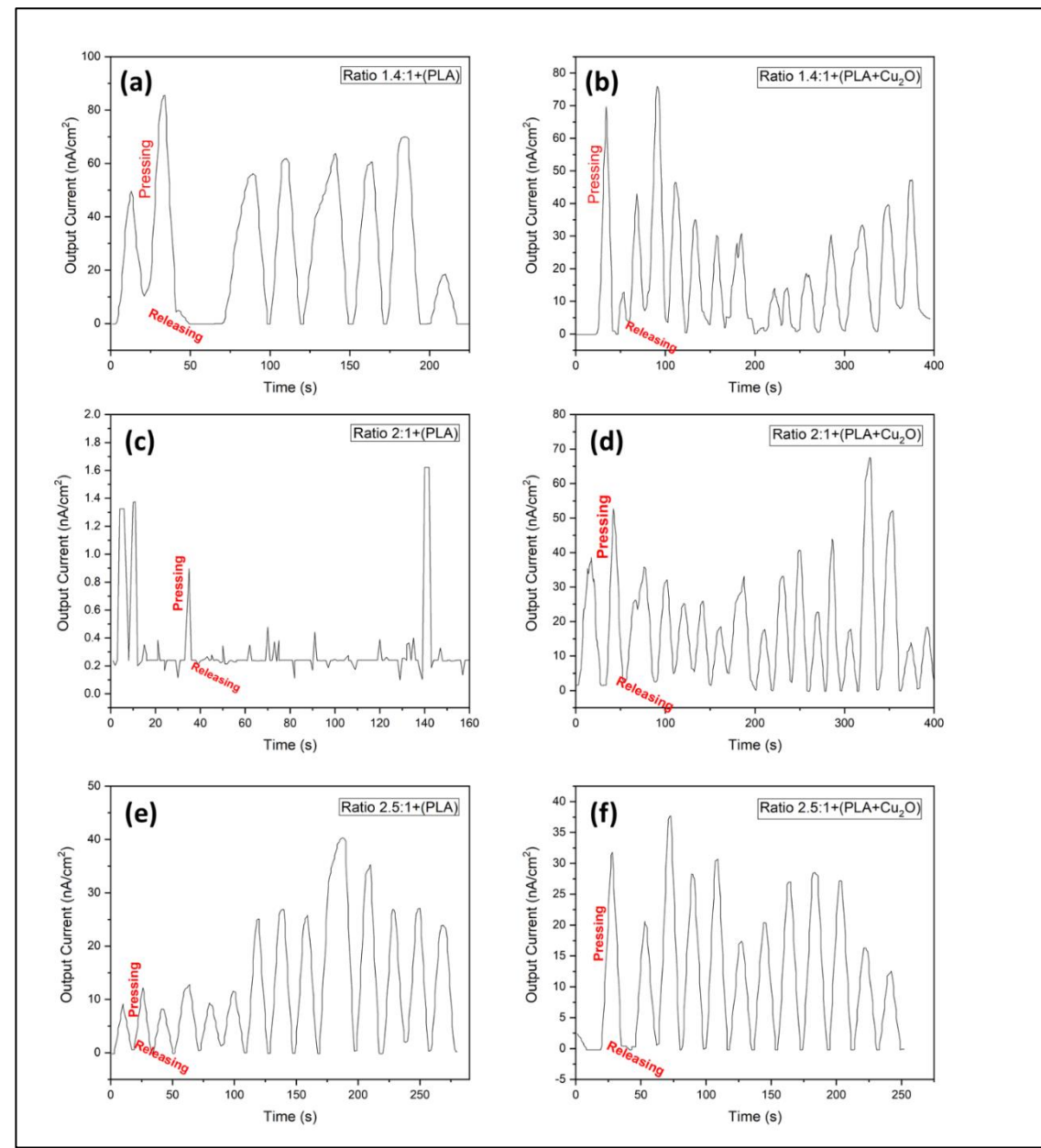


Figure 8
Measurement of
Current versus Time
in a Nanogenerator
Device with Ratio
Comparison. a) Ratio
1.4:1+(PLA), b) Ratio
1.4:1+(PLA+Cu2O), c)
Ratio 2:1+ (PLA), d)
Ratio 2:1+ (PLA +
Cu2O), e) Ratio 2.5:1
+ (PLA), f) Ratio 2.5:1
+ (PLA) + Cu<sub>2</sub>O)

This is because PLA polymer has an important role in this device. First, passivates ZnO nanorods and reduces the formation of film coating due to chemical absorption (chemisorption). These passivates improve the performance of the nanogenerator. Then, capillary force and force applied due to weight cause current to flow into the nanorods and fill the gaps between the nanorods. Pressure is applied to generate strain along the growth direction of the ZnO and generate a resulting piezo potential gradient from the root to the top of the nanorods. The same potential gradient is generated from the top and bottom sides of the substrate. This potential difference drives the transient inductance flow.

Table 6. Current Measurements in Piezoelectric Nanogenerators

Ratio comparison	Mass (kg)	Weight (N)	P (N/m <sup>2</sup> )	Current ± 0.01 (nA)
1.4:1+(PLA)				85
2:1 + PLA	5.9	57.82	29.5	1.6
2,5:1+(PLA)				39
1,4:1+(PLA+Cu <sub>2</sub> O)				76
2:1+(PLA+Cu <sub>2</sub> O)				67
2.5:1+(PLA+Cu <sub>2</sub> O)				37.5

## 3.4.2 Voltage Characterization (V)

The voltage characteristic (V) in piezoelectric devices is carried out with emphasis, because of the ability of this material to produce an electric field or electric potential in response to mechanical pressure. The performance of the nanogenerator produced by mechanical strength per area was measured and the results are shown in Figure 9.

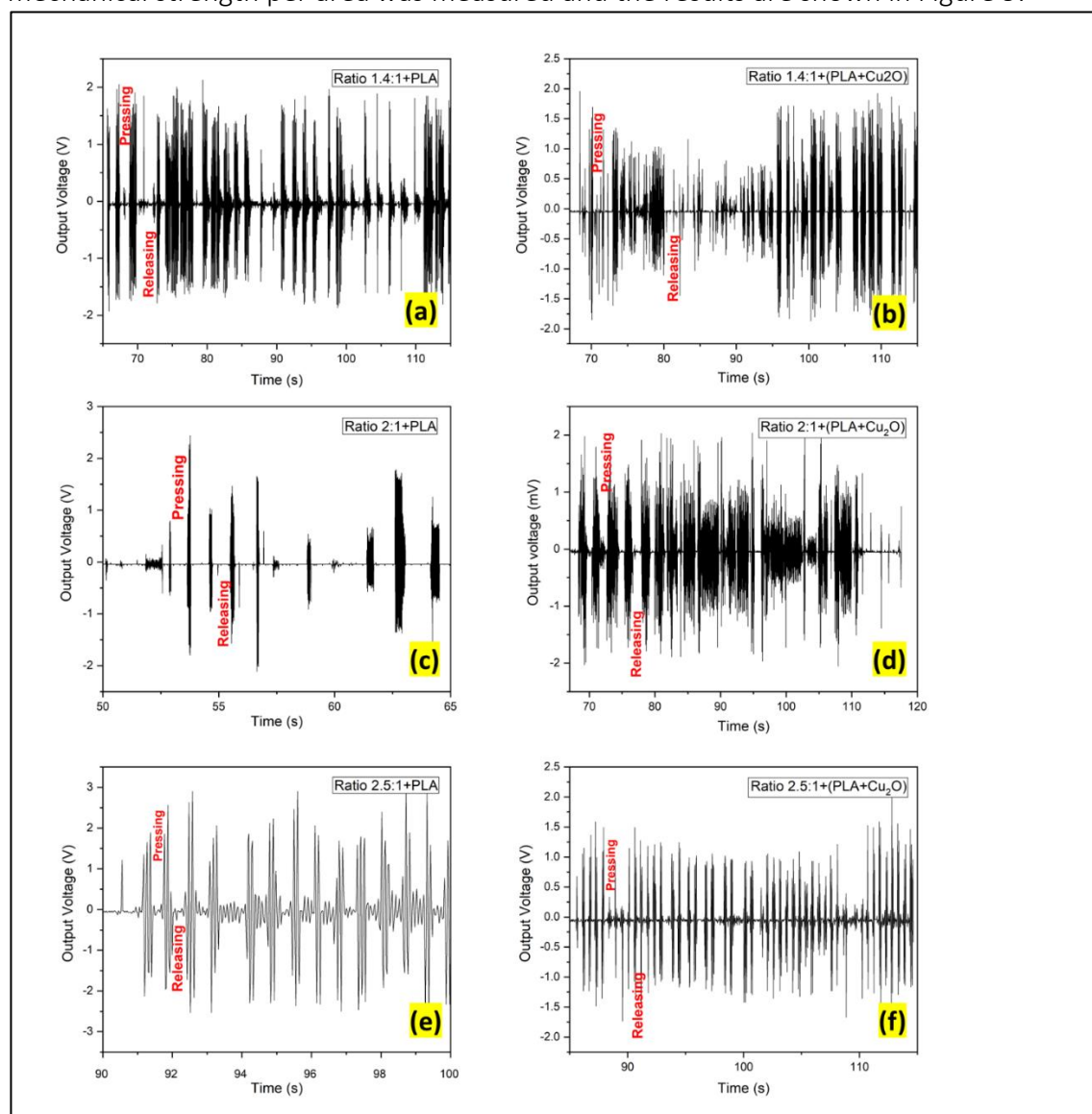


Figure 9
Measurement of
voltage versus time
on a nanogenerator
device with ratio
comparison. a) Ratio
1.4:1+(PLA), b) Ratio
1.4:1+(PLA+Cu2O), c)
Ratio 2:1+(PLA), d)
Ratio 2:1+ (PLA +
Cu<sub>2</sub>O), e) Ratio 2.5:1+
(PLA), f) Ratio 2.5:1+
(PLA+Cu<sub>2</sub>O)

Figure 9 shows that the response obtained from the nanogenerator is due to the dynamic force of the human finger/hand per area. The maximum voltage generated in the best piezoelectric nanogenerator device was found to reach 3 V at a ratio of 2.5:1+(PLA). This shows that PLA film has an important role in nanogenerator performance compared to PLA/Cu2O film. The voltage results that show a good response can be seen in more detail in Table 7.

Table 7. Voltage Measurements in Piezoelectric Nanogenerator

Ratio Comparison	Mass (kg)	Weight (N)	P (N/m²)	Voltage ± 0.01 V
1,4:1 + PLA				2,2
2:1+(PLA)				2,4
2,5:1+(PLA)				3,0
1,4:1+(PLA+Cu <sub>2</sub> O)	3,1	30,38	6,1	1,9
2:1+(PLA+Cu2O)				2,1
2,5:1+(PLA+Cu <sub>2</sub> O)				2,0

The human body contains large amounts of energy in the form of heat energy, fat, and kinetic energy from body movement. Attracting the attention of researchers by utilizing wasted energy in the surrounding environment, it is now starting to be developed. The development of low-power electronic devices makes it possible to use humans as self-powered systems to power electronic devices. We have measured the output power produced by the nanogenerator under pressing and releasing conditions. The performance of the artificial nanogenerator device (active area 1 x 2 cm2) was tested by fixing the device above and below the finger to harvest energy from pressure.

Asymmetric piezoelectric potential and Schottky contact between electrodes, ZnO nanorods and polymer layers are key factors for creating, separating, preserving, accumulating and discharging charge [22]. Stainless steel (SS) used as a substrate not only increases conductivity as an electrode but is resistant to mechanical stress and anticorrosion. In practice, this device becomes like a battery with a positive charge on its surface when pressed and a negative charge when relaxed / no pressure is applied with the force applied. The force is obtained by measuring and estimating the pressure on the hand/finger that is pressed with the balance of weight and the number of gravitational speeds  $g = 9.8 \text{ m/s}^2$ .

Figures 8 and 9 show that the physical principles behind the discharge energy in piezoelectric devices arise from how the piezoelectric and semiconductor properties of ZnO are combined. Changes in the shape of ZnO nanorods cause a strain field along the nano rod, the outer surface is stretched ( $+\epsilon$ ) and the inner surface is compressed ( $-\epsilon$ ), so when the strain is positive ( $+\epsilon$ ) it causes a positive electric field ( $+\epsilon$ ). When a collective electric field occurs in each nanorod, the collective electric field between all the nanorods will create an electric field that depends on the nano-rods.

## 4. Conclusion

Based on the results of the research and data analysis that has been carried out, it can be concluded as follows. First is ZnO *nanorods* successfully synthesized using the hydrothermal method with ZnO nanoparticles as the buffer layer. The crystal structure formed is hexagonal wurtzite with the highest orientation in the (002) plane towards the c-axis. The greater the precursor concentration, the larger the resulting grain size. However, in this study ZnO nanorods with a ratio of 1.4:1 to a ratio of 2:1 experienced a decrease in crystal grain size, while at a ratio of 2.5:1 it increased. The precursor concentration affects the length and diameter of the resulting nanorods. The greater the precursor concentration, the larger the rods produced. In this research, good surface morphology of ZnO nanorods was obtained at a ratio of 1.4:1 and ratio 2.5:1, with diameters of 81.568 and 80.429 respectively.

Dielectricity measurements on samples of ZnO nanorods, PLA film, and PLA/Cu2O film using an LCR Meter which shows the relationship between the dielectric constant value and frequency. The greater the given frequency, the dielectric constant decreases. The frequency range is 100000 Hz-200000 Hz at a ratio of 1.4:1+(PLA) and ratio 2:1+(PLA+Cu2O). The dielectric constant value tends to be random, this is because the polarization ability of the dielectric material changes according to the given frequency. This dielectric property describes the level of a material's ability to store electric charge at a high potential difference. Suitability of application in harvesting energy, the nanogenerator uses pressure on the finger/hand of approximately 29.5 N with a mass of 5.9 kg to the greatest current occurring at a ratio of 1.4:1+(PLA) with I max = 85 nA. Meanwhile, the greatest voltage produced is found at a ratio of 2.5:1+(PLA) with V max =

Publisher: Tinta Emas Institute

3 volts with a pressure force used of 6.1 N with a mass of 3.1 kg. The greater the mass or pressure force used, the greater the current and voltage produced.

# 5. Author's Declaration

**Author contributions and responsibilities -** The authors made major contributions to the conception and design of the study. The authors took responsibility for data analysis, interpretation and discussion of results. The authors read and approved the final manuscript.

**Funding** - This research did not receive external funding.

Availability of data and materials - All data is available from the author.

Competing interests - The authors declare no competing interests.

**Did you use generative AI to write this manuscript? - I** do not use AI assistance in my manuscript.

Declaration of generative AI and AI-assisted technologies in the writing process - During the preparation of this work the author did not use AI to write, edit, or other things related to the manuscript.

# 6. References

- [1] H. E. Colak, T. Memisoglu, and Y. Gercek, 'Optimal site selection for solar photovoltaic (PV) power plants using GIS and AHP: A case study of Malatya Province, Turkey', *Renewable Energy*, vol. 149, pp. 565–576, Apr. 2020, doi: 10.1016/j.renene.2019.12.078.
- [2] P. A. Christensen *et al.*, 'Risk management over the life cycle of lithium-ion batteries in electric vehicles', *Renewable and Sustainable Energy Reviews*, vol. 148, p. 111240, 2021.
- [3] A. dos Santos *et al.*, 'Optimization of ZnO Nanorods Concentration in a Micro-Structured Polymeric Composite for Nanogenerators', *Chemosensors*, vol. 9, no. 2, Art. no. 2, Feb. 2021, doi: 10.3390/chemosensors9020027.
- [4] A. T. Le, M. Ahmadipour, and S.-Y. Pung, 'A review on ZnO-based piezoelectric nanogenerators: Synthesis, characterization techniques, performance enhancement and applications', *Journal of Alloys and Compounds*, vol. 844, p. 156172, Dec. 2020, doi: 10.1016/j.jallcom.2020.156172.
- [5] S. Vendoti, M. Muralidhar, and R. Kiranmayi, 'Techno-economic analysis of off-grid solar/wind/biogas/biomass/fuel cell/battery system for electrification in a cluster of villages by HOMER software', *Environ Dev Sustain*, vol. 23, no. 1, pp. 351–372, Jan. 2021, doi: 10.1007/s10668-019-00583-2.
- [6] K. Batra, N. Sinha, and B. Kumar, 'Ba-doped ZnO nanorods: Efficient piezoelectric filler material for PDMS based flexible nanogenerator', *Vacuum*, vol. 191, p. 110385, Sep. 2021, doi: 10.1016/j.vacuum.2021.110385.
- [7] N. Jayababu and D. Kim, 'ZnO nanorods@conductive carbon black nanocomposite based flexible integrated system for energy conversion and storage through triboelectric nanogenerator and supercapacitor', *Nano Energy*, vol. 82, p. 105726, Apr. 2021, doi: 10.1016/j.nanoen.2020.105726.
- [8] S. Rafique, A. K. Kasi, J. K. Kasi, Aminullah, M. Bokhari, and Z. Shakoor, 'Fabrication of silver-doped zinc oxide nanorods piezoelectric nanogenerator on cotton fabric to utilize and optimize the charging system', *Nanomaterials and Nanotechnology*, vol. 10, p. 1847980419895741, Jan. 2020, doi: 10.1177/1847980419895741.
- [9] L. Ye *et al.*, 'High-performance piezoelectric nanogenerator based on electrospun ZnO nanorods/P(VDF-TrFE) composite membranes for energy harvesting application', *J Mater Sci: Mater Electron*, vol. 32, no. 4, pp. 3966–3978, Feb. 2021, doi: 10.1007/s10854-020-05138-0.
- [10] S. Bairagi and S. W. Ali, 'A hybrid piezoelectric nanogenerator comprising of KNN/ZnO nanorods incorporated PVDF electrospun nanocomposite webs', *International Journal of Energy Research*, vol. 44, no. 7, pp. 5545–5563, 2020, doi: 10.1002/er.5306.

- [11] A. Taufiq *et al.*, 'Effects of ZnO nanoparticles on the antifungal performance of Fe3O4/ZnO nanocomposites prepared from natural sand', *Advances in Natural Sciences: Nanoscience and Nanotechnology*, vol. 11, no. 4, p. 045004, 2020.
- [12] S. Park, S. Choi, K. Kim, W. Kim, and J. Park, 'Effects of ammonium perchlorate particle size, ratio, and total contents on the properties of a composite solid propellant', *Propellants, Explosives, Pyrotechnics*, vol. 45, no. 9, pp. 1376–1381, 2020.
- [13] C. Arif, B. I. Setiawan, S. K. Saptomo, M. Taufik, S. F. D. Saputra, and M. Mizoguchi, 'Functional design of smart evaporative irrigation for mina-padi system in Indonesia', in *IOP Conference Series: Earth and Environmental Science*, IOP Publishing, 2021, p. 012052.
- [14] R. Maity, A. Dutta, S. Halder, S. Shannigrahi, K. Mandal, and T. P. Sinha, 'Enhanced photocatalytic activity, transport properties and electronic structure of Mn doped GdFeO 3 synthesized using the sol–gel process', *Physical Chemistry Chemical Physics*, vol. 23, no. 30, pp. 16060–16076, 2021.
- [15] N. Mufti, S. Maryam, A. Sari Puspita Dewi, A. Taufiq, R. Kurniawan, and Sunaryono, 'The effect of Zn-acetate molar variation on phase formation and photocatalytic degradation activity of Fe3O4/ZnO core-shell nanocomposite', *Molecular Crystals and Liquid Crystals*, vol. 694, no. 1, pp. 49–59, 2019.
- [16] S. Mojtahedi, M. Karimipour, E. Heydari-Bafrooei, and M. Molaei, 'Application of ascorbic acid in the synthesis of rGO/micro-octahedral Cu2O nanocomposites and its effect on the wide linear response range of glucose detection', *Microchemical Journal*, vol. 159, p. 105405, Dec. 2020, doi: 10.1016/j.microc.2020.105405.
- [17] E. Handoko *et al.*, 'Complex permittivity, permeability and microwave absorption studies of double layer magnetic absorbers based on BaFe12O19 and BaFe10CoZnO19', in *Materials Science Forum*, Trans Tech Publ, 2019, pp. 302–307.
- [18] S. S. Naik, S. J. Lee, T. Begildayeva, Y. Yu, H. Lee, and M. Y. Choi, 'Pulsed laser synthesis of reduced graphene oxide supported ZnO/Au nanostructures in liquid with enhanced solar light photocatalytic activity', *Environmental Pollution*, vol. 266, p. 115247, Nov. 2020, doi: 10.1016/j.envpol.2020.115247.
- [19] S. Rani, S. Kapoor, B. Sharma, S. Kumar, R. Malhotra, and N. Dilbaghi, 'Fabrication of Zn-MOF@rGO based sensitive nanosensor for the real time monitoring of hydrazine', *Journal of Alloys and Compounds*, vol. 816, p. 152509, Mar. 2020, doi: 10.1016/j.jallcom.2019.152509.
- [20] G. A. Bowmaker, Y. Kim, B. W. Skelton, A. N. Sobolev, and A. H. White, 'Structures of 1:1 Mononuclear Adducts of Zinc(ii) Halides, ZnX2 (X = Cl, Br, I) and of New Hydrates of 1:1 Adducts of Zinc(ii) Nitrate and Sulfate with Aromatic N,N"-Bidentate Base Derivatives of Pyridine (bpy, phen)', Aust. J. Chem., vol. 73, no. 6, pp. 511–519, Nov. 2019, doi: 10.1071/CH19365.
- [21] Z. Wang *et al.*, 'Optimizing the Oxygen-Catalytic Performance of Zn–Mn–Co Spinel by Regulating the Bond Competition at Octahedral Sites', *Advanced Functional Materials*, vol. 33, no. 16, p. 2214275, 2023, doi: 10.1002/adfm.202214275.
- [22] Q. He, X. Li, J. Zhang, H. Zhang, and J. Briscoe, 'P–N junction-based ZnO wearable textile nanogenerator for biomechanical energy harvesting', *Nano Energy*, vol. 85, p. 105938, Jul. 2021, doi: 10.1016/j.nanoen.2021.105938.